ELECTRON TRANSPORT MECHANISM IN A HALL THRUSTER

Miharu Hirakawa*
Tokai University
Hiratsuka-shi, Kanagawa, JAPAN

Abstract

The plasma fluctuation and its effect on the electron transport in the acceleration channel of a Hall thruster were investigated. The existence of the plasma fluctuation was examined using the particle simulation method where both ions and electrons are treated as particles. The simulation result also showed that the oscillating electric field can raise the electron mobility normal to the magnetic field lines. To understand the mechanism of the fluctuation observed in the simulation, electron and ion behavior was analytically discussed using the equations of continuity and motion.

Nomenclature
(SI units unless noted otherwise)

- B : magnetic flux density
- E : electric field
- e : electronic charge
- I_a : discharge current
- Kn : Knudsen number at the orifice
- k : wave number vector
- k_B : Boltzmann's constant
- L : acceleration channel length
- m : particle mass
- n : number density
- q : particle charge
- r : distance from the center line of the thruster
- r_1, r_2 : inner and outer radii of the acceleration channel
- $\bar{r}$: average radius of the acceleration channel
- S : cross section of the channel
- T : temperature
- t : time
- V_a : discharge voltage
- v : velocity
- x : the direction the wave propagates
- α : phase lag of the density
- β : phase lag of the velocity
- δ : secondary-electron emission yield of the surface
- ε_0 : permittivity of vacuum
- ϕ : space potential
- γ : ratio of electron cyclotron frequency to plasma frequency
- ν : collision frequency
- θ : azimuthal angle
- σ : collisional cross section
- ω : angular frequency of the plasma oscillation
- ω_{ce}, ω_{ci}: cyclotron frequencies
- ω_{pe}, ω_{pi}: plasma frequencies

Subscripts

- e : electron
- i : ion
- ion : ionization collision
- n : neutral atom
- r, θ, z : cylindrical coordinate directions
- x, y, z : Cartesian coordinate directions
- 0 : representative value/equilibrium quantity
- 1 : perturbation quantity
- $< >$: average

Superscripts

- $\tilde{(\ )}$: dimensionless quantity
- $\bar{(\ )}$: complex amplitude

Introduction

Electron motion across the magnetic fields have the effects on the discharge characteristics and the thruster performance of Hall thrusters owing to the magnetic field configuration in their acceleration channel. In general, it is empirically known that in a large magnetic field observed electron mobility and diffusion coefficient normal to the magnetic field are larger than values calculated on the assumption of "classical diffusion" caused by collisions of electrons with heavy particles. From the theoretical estimation of the discharge characteristics of a Hall thruster, it was found that the result based on the Bohm diffusion theory—that is one of the anomalous diffusion theory—is much closer to experiment than that based on the classical diffusion theory. The "anomalous diffusion" is explained by the theory that the scattering of electrons by the walls can play a role analogous to the scattering of electrons by neutral atoms and ions in

* Assistant Professor, Department of Aeronautics and Astronautics, Member AIAA.

the acceleration channel[1]. In an another theory, it is stated that turbulence in the plasma causes electron "anomalous diffusion"[2,3]. This theory predicts that electrons come to more easily run toward the anode across the radial magnetic field lines if plasma fluctuation occurs in the acceleration channel of Hall thrusters.

Thus, the objective of this work is to investigate the plasma fluctuation and its effect on the electron transport in the Hall thruster. The particle simulation method is used to examine the existence of the plasma fluctuation. Referring to the simulation results, the mechanism of the plasma fluctuation is analytically discussed using the equation of continuity and the fluid equation of motion.

Particle Simulation of Plasma Fluctuation

Simulation method

The block diagram of the particle simulation code used here is shown in Fig. 1. This code includes a charged particle simulation based on the Particle-in-Cell(PIC) coupled with the Monte Carlo method.

In this simulation, both ions and electrons are treated as particles. The trajectories of many test particles are followed using the Newton-Lorentz equation:

$$m\frac{dv}{dt} = q(E + v \times B) \tag{1}$$

Once positions and velocities of all test particles are determined, the spatial distributions of electron and ion densities, velocities and energies can be calculated. As this simulation presumes the electrostatic approximation:

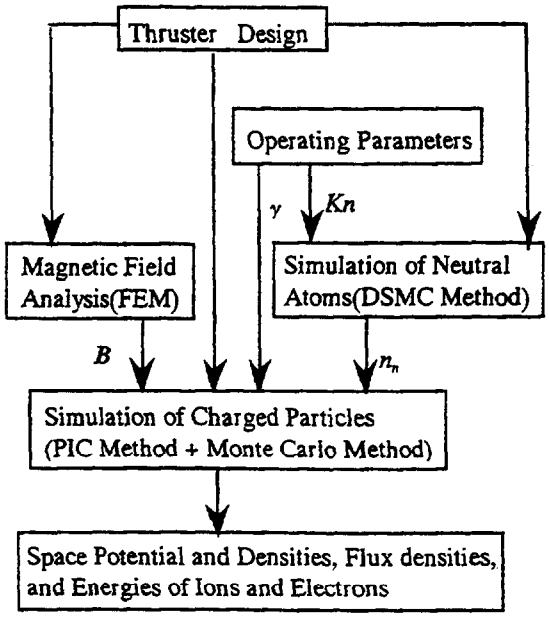

Fig. 1 Block diagram of the particle simulation.

$$E = -\nabla\phi\ , \tag{2}$$

the electric field is found self-consistently on each computational cycle, while the magnetic field is given before. The space potential is obtained by solving the Poisson equation:

$$\Delta\phi = -\frac{e}{\varepsilon_0}(n_i - n_e), \tag{3}$$

where we neglect multi-charged ions. Rewriting the above equations Eqs. (1) - (3), it becomes clear that the frequency ratio γ, that is the ratio of electron cyclotron frequency ω_{ce} to plasma frequency ω_{pe}, has a significant effect on the plasma behavior[4]. These two frequencies, ω_{ce} and ω_{pe}, are defined by the following equations:

$$\omega_{ce} = \frac{eB_0}{m_e}, \tag{4}$$

$$\omega_{pe} = \sqrt{\frac{n_0 e^2}{\varepsilon_0 m_e}}, \tag{5}$$

where n_0 and B_0 are representative values of the electron density and the magnetic flux density. The discharge current I_a —the number of test particles emitted from the cathode is determined from this current—being given as an input parameter, the discharge voltage is automatically determined. Hence, I_a and B_0 should be chosen so that γ agrees with the actual value to make up the condition that the smaller mass ratio of 1840 and lower density than actual values are used in the simulation.

The author has assumed that ion motion is not affected by collisions with particles because of the mean free path for ion-ion and ion-atom collisions longer than the acceleration channel length. As for electrons, the following three kinds of collisions are taken into account: 1) elastic collision with neutral atoms, 2) elastic collision with ions, and 3) inelastic collision with neutral atoms such as ionization collisions and excitation collisions. When an ionization collision occurs, a pair of an ion and a low-energy electron is produced. As a result, the ion production rate is automatically determined through the simulation. The procedure of this simulation is described in detail in Ref. 4 and 5.

The cylindrical coordinate system is taken where r is the distance from the thruster axis, along which z extends downstream. When the plasma fluctuation resulting in the azimuthal variation is treated, the simulation region is restricted within a toroidal acceleration channel with square cross section as shown in Fig. 2; solving Eq. (3) with a given axial

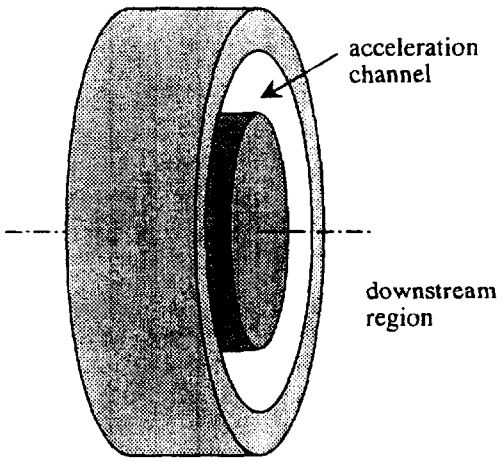

Fig. 2 Simulation region.

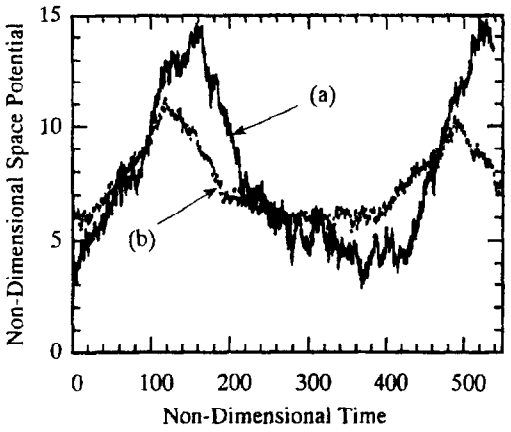

Fig. 4 Oscillation of the space potential at one position on the same condition as in Fig. 3 when the wall potential is (a) floating and (b) fixed.

electric field for the space potential yields its distribution in the r-θ plane. To examine the axial distribution of plasma or to investigate the plume profiles, the region is not limited to the channel exit but extended to its downstream region out of the channel; Eq. (3) is solved to obtain the space potential distribution in the r-z plane.

Simulation results

A particle simulation was performed in a given constant axial electric field $E_z = V_a / L$. Some results show the plasma oscillations as in Figs. 3-6. In the following results, values will be written in the dimensionless units, where time is measured in units of $1/\omega_{pe}$, potential in units of the electron temperature near the cathode $k_B T_e / e$, density in units of the representative density n_0, and velocities in units of the electron thermal velocity $\sqrt{k_B T_e / m_e}$. The space potential changes along the azimuth as in Fig. 3 and with time as in Fig. 4. These results indicate that the plasma wave propagates in the azimuthal direction, which is the same direction as the vector product of the applied axial electric field and the radial magnetic field. Two curves in these figures correspond to different boundary conditions on the channel walls, showing no significant qualitative difference. In these cases, the period of the fluctuation is about $400/\omega_{pe}$ and $k_\theta \bar{r}$ is 4 or 5. Densities and azimuthal velocities vary in the azimuthal direction with the phase difference as shown in Figs. 5 and 6, oscillating with time. The average azimuthal ion velocity is four orders of magnitude smaller than the electron velocity, which is close to the $\boldsymbol{E} \times \boldsymbol{B}$ drift velocity induced by the axial electric field and radial magnetic field. Accordingly, it was confirmed that ions are exhausted before their orbits are effected by the magnetic field. From the obtained azimuthal distributions, we can roughly estimate the axial

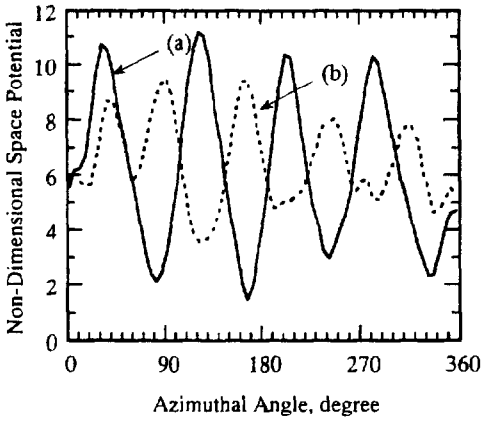

Fig. 3 Space potential distributions at $r = \bar{r}$ obtained by the particle simulation (L=8 mm, r_1=19 mm, r_2=25 mm, γ=1.0, K_n=0.3, and V_a=50 V), when the wall potential is (a) floating and (b) fixed.

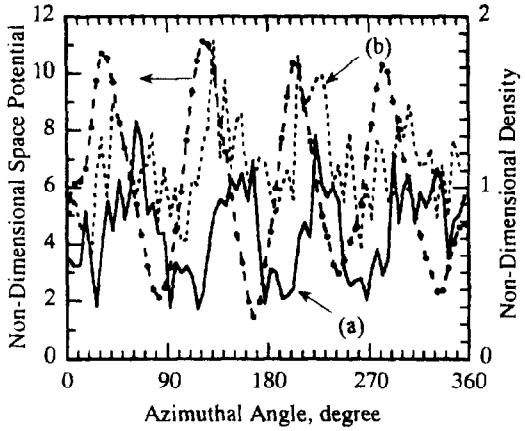

Fig. 5 Distributions of the space potential and densities of (a) electron and (b) ion obtained by the particle simulation on the same condition as Fig. 3(a).

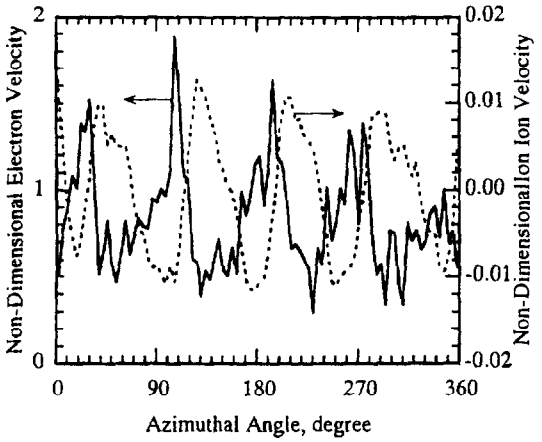

Fig. 6 Azimuthal velocity distributions of (a) electron and (b) ion obtained by the particle simulation on the same condition as Fig. 3(a).

electron flux caused by the interaction between the radial magnetic field and an induced azimuthal electric field. The calculated axial electron mobility is in the range of $1/18B_r \sim 1/16B_r$ [5], which nearly agrees with the mobility based on the Bohm diffusion, $1/16\,B_r$.

Analysis of Plasma Wave

The plasma wave was analytically discussed to understand the mechanism of the fluctuation observed in the above simulation. The equation of continuity and the fluid equation of motion were used:

$$\frac{\partial n}{\partial t} + \nabla(nv) = n_e n_n \langle \sigma v \rangle_{ion} \tag{6}$$

$$m\left[\frac{\partial v}{\partial t} + (v\cdot\nabla)v\right] = q(-\nabla\phi + v\times B) - \frac{k_B T}{n}\nabla n - mvv \tag{7}$$

Separating the dependent variables into two parts: "equilibrium" part indicated by a subscript 0, and a "perturbation" part indicated by a subscript 1:

$$n = n_0 + n_1\ , \tag{8}$$

$$v = v_0 + v_1\ , \tag{9}$$

$$\phi = \phi_0 + \phi_1\ . \tag{10}$$

As for ions, their temperature and collisions being neglected, Eqs. (6) and (7) are linearized as

$$\frac{\partial n_{i1}}{\partial t} + \nabla(n_{i0}v_{i1} + n_{i1}v_{i0}) = n_{e1}n_n\langle\sigma v\rangle_{ion}\ , \tag{11}$$

$$m_i\left[\frac{\partial v_{i1}}{\partial t} + v_{i1}\cdot\nabla v_{i0} + v_{i0}\cdot\nabla v_{i1}\right] = e(-\nabla\phi_1 + v_{i1}\times B)\ . \tag{12}$$

Any oscillating quantity — say, the density — is assumed to behave sinusoidally:

$$n_1 = \bar{n}_1 \exp[i(k\cdot r - \omega t)] \tag{13}$$

We shall consider the Cartesian coordinates of which x axis lies along k. The x, y, and z directions correspond to the azimuthal, axial, and radial directions in the thruster. Then, oscillating quantities are expressed as

$$v_1 = \bar{v}_1 \exp[i(k_x x - \omega t)], \tag{14}$$

$$n_1 = \bar{n}_1 \exp[i(k_x x - \omega t)], \tag{15}$$

$$\phi_1 = \bar{\phi}_1 \exp[i(k_x x - \omega t)]. \tag{16}$$

Substituting these in Eq. (11) and taking into consideration that the equilibrium quantities are uniform in the x direction, we have

$$-i\omega\bar{n}_{i1} + ik_x\bar{n}_{i0}\bar{v}_{i1x} + \bar{v}_{i1y}\frac{\partial n_{i0}}{\partial y} + \bar{n}_{i1}\frac{\partial v_{i0y}}{\partial y} + ik_x\bar{n}_{i1}v_{i0x} = \bar{n}_{e1}n_n\langle\sigma v\rangle_{ion} \tag{17}$$

On the assumption that the azimuthal velocity v_{i0x} and the axial component of the magnetic field B_y are negligible, the components of Eq. (12) are now

$$m_i(-i\omega + \partial_y v_{i0y})\bar{v}_{i1x} = e(-k_x\bar{\phi}_1 + \bar{v}_{i1y}B_z), \tag{18}$$

$$m_i[(-i\omega + \partial_y v_{i0y})\bar{v}_{i1y} + ik_x\bar{v}_{i1x}v_{i0y}] = -e\bar{v}_{i1x}B_z\ , \tag{19}$$

where $\partial_y v_{i0y}$ expresses $\partial v_{i0y}/\partial y$. In addition, we also neglect the density gradient $\partial n_{i0}/\partial y$ and adopt the following condition because of the periodicity of the oscillating electric field on inner and outer channel walls:

$$|\bar{n}_{e1}| = |\bar{n}_{i1}|\ . \tag{20}$$

Consequently, Eq. (17) can be arranged as

$$\bar{n}_{i1} = \frac{-k_x n_{i0}}{-\omega - i\partial_y v_{i0y} + in_n\langle\sigma v\rangle_{ion}}\bar{v}_{i1x} \tag{21}$$

The term of $in_n\langle\sigma v\rangle_{ion}$ will be neglected after this, since it is much lower than the frequency of the wave observed in the simulation. Eliminating v_{i1y} from Eqs. (18) and (19), we obtain

$$\bar{v}_{i1x} = \frac{1}{m_i}\frac{(\omega + i\partial_y v_{i0y})ek_x\bar{\phi}_1}{G + iH} \tag{22}$$

$$= \sqrt{\frac{\omega^2 + (\partial_y v_{i0y})^2}{G^2 + H^2}}\frac{ek_x}{m_i}\exp(-i\beta_i)\bar{\phi}_1\ , \tag{23}$$

where

$$G = \omega^2 - \left(\partial_y v_{i0y}\right)^2 - {\omega_{ci}}^2 , \quad (24)$$

$$H = 2\omega\partial_y v_{i0y} - \omega_{ci} k_x v_{i0y} . \quad (25)$$

The phase lag of the ion velocity from the space potential, β_i, is expressed by

$$\beta_i = \tan^{-1}\left(\frac{H}{G}\right) - \tan^{-1}\left(\frac{\partial_y v_{i0y}}{\omega}\right). \quad (26)$$

Substituting Eq. (23) into Eq. (21), we have

$$\bar{n}_{i1} = \frac{e{k_x}^2 n_{i0}}{m_i\sqrt{G^2+H^2}}\exp(-i\alpha_i)\bar{\phi}_1 , \quad (27)$$

where the phase lag of the ion density from the potential, α_i, is described as

$$\alpha_i = \tan^{-1}\left(\frac{H}{G}\right) \quad (28)$$

Considering that ions are accelerated in the y direction by the discharge voltage V_a, we can make an approximation that $v_{i0y} = (4/9)\sqrt{2eV_a/m_i}$ and $\partial_y v_{i0y} = \sqrt{2eV_a/m_i}/L$. The coefficient of v_{i0y} was calculated on the assumption of the uniform ionization in the channel. Using these equations and inserting m_i, B_z, n_{i0}, V_a, k_x, and ω, we can calculate ion density and velocity from Eqs. (23) -(28). For example, $\left|\tilde{\bar{n}}_{i1}\right| = 0.1$, $\left|\tilde{\bar{v}}_{i1x}\right| = 0.014$, $\alpha_i = 45\,\text{deg.}$, $\beta_i = 22\,\text{deg.}$ were obtained with the same input parameters, wave number, and frequency as in Figs. 5 and 6. These are close to the following values read from above figures except the ion density amplitude: $\left|\tilde{\bar{n}}_{i1}\right| = 0.3$, $\left|\tilde{\bar{v}}_{i1x}\right| = 0.01$, $\alpha_i/(k_\theta \bar{r}) = 10-20\,\text{deg.}$, and $\beta_i/(k_\theta \bar{r}) = 5-15\,\text{deg.}$, where $k_\theta \bar{r} = 4$.

As for electrons, linearization of the continuity equation leads to the equation:

$$-i\omega\bar{n}_{e1} + ik_x n_{e0}\bar{v}_{e1x} + \bar{v}_{e1y}\frac{\partial n_{e0}}{\partial y} + \bar{n}_{e1}\frac{\partial v_{e0y}}{\partial y} + ik_x\bar{n}_{e1}v_{e0x} = \bar{n}_{e1}n_n\langle\sigma v\rangle_{ion} \quad (29)$$

When the average axial velocity of electron v_{e0y} is assumed to be constant (that is approximately equal to $-I_a/eSn_{e0}$), the above equation can be arranged as

$$\bar{n}_{e1} = \left|\bar{n}_{e1}\right|\exp(-i\alpha_e) = \frac{k_x n_{e0}}{\omega - k_x v_{e0x}}\bar{v}_{e1x} . \quad (30)$$

From this equation, it is indicated that the phase difference between the electron density and the velocity is 0 for $\omega > k_x v_{e0x}$ and π for $\omega < k_x v_{e0x}$, which tendency is recognized in the result of particle simulation (Figs. 5 and 6).

The equation of motion Eq. (7) is arranged as

$$m_e\left[\frac{\partial v_{e1}}{\partial t} + v_{e1}\cdot\nabla v_{e0} + v_{e0}\cdot\nabla v_{e1}\right] = -e\left(-\nabla\phi_1 + v_{e1}\times B\right) - \frac{k_B T_e}{n_{e0}}\nabla n_{e1} - mv_{e1}\nu . \quad (31)$$

Using the same procedure as for ions and adopting the condition $k_B T_e \ll e\bar{\phi}_1$, the velocity is described by the equation:

$$\bar{v}_{e1x} = \frac{1}{m_e}\frac{ek_x(\omega + i\nu)\bar{\phi}_1}{J + iK} \quad (32)$$

$$= \sqrt{\frac{\omega^2+\nu^2}{J^2+K^2}}\frac{ek_x}{m_e}\exp(-i\beta_e)\bar{\phi}_1 , \quad (33)$$

where

$$\beta_e = \tan^{-1}\left(\frac{K}{J}\right) - \tan^{-1}\left(\frac{\nu}{\omega}\right), \quad (34)$$

$$J = -\omega^2 + \nu^2 + k_x v_{e0x}\omega + {\omega_{ce}}^2 , \quad (35)$$

$$K = -2\omega\nu + k_x v_{e0x}\nu + \omega_{ce}k_x v_{e0y} . \quad (36)$$

From these, $\left|\bar{v}_{e1x}\right|$ is calculated to be about 10^{-2} of the electron thermal velocity, which is less than 0.1 of the velocity seen in Fig. 6. Consequently, Eq. (31) is thought not appropriate to describe this fluctuation.

When the ion axial velocity v_{i0y} remains constant, the wave frequency can be analytically obtained from the electron and ion equations of continuity and motions as follows[6,7]:

$$\omega = k_y v_{i0y} \pm \sqrt{\frac{(k_x v_{e0x})^2 - {\omega_{ce}}^2}{(k_x v_{e0x})^2 - {\omega_{ce}}^2 - {\omega_{pe}}^2}}\omega_{pi} . \quad (37)$$

The calculated frequency is the same order of magnitude as that of the plasma fluctuation in Fig. 3-6. However, this may be not valid in this work, since this is derived using the electron fluid equation of motion as well as Eq. (33).

Considering the above disagreement in $\left|\bar{v}_{e1x}\right|$, it is required to introduce the influence of the interaction between electrons and walls. However, this phenomenon probably cannot be expressed by the fluid equation. Accordingly, the author decided to use the particle simulation for investigation of the electron behavior in an oscillating electric field. Electric and

magnetic fields being given, the trajectories of many electrons in the channel are calculated using the Newton-Lorentz equation Eq. (3); spatial distributions of density and velocity are obtained from their positions and velocities. For simplicity, the axial magnetic field and collisions between particles are neglected. While the axial electric field is kept uniform and constant, the radial and azimuthal electric fields are determined by the following pseudo-potentials:

$$\phi = \phi_0 + \bar{\phi}_{1m} \cos(k_\theta \bar{r}\theta - \omega t) . \quad (38)$$

$$\phi = \phi_0 \sin\left(\frac{r - r_1}{r_2 - r_1}\pi\right) + \bar{\phi}_{1m} \cos(k_\theta \bar{r}\theta - \omega t), \quad (39)$$

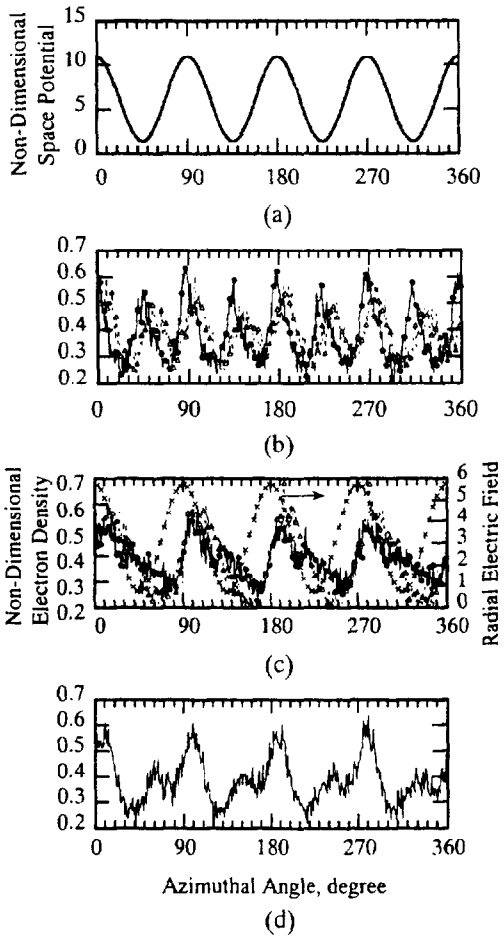

Fig. 7 Distributions of (a) the space potential in the middle of the channel ($\tilde{\phi}_0 \approx 6$, $\tilde{\bar{\phi}}_{1m} \approx 5$, $k_\theta \bar{r} = 4$, $\tilde{\omega} = 2\pi/380$) and (b)-(d) electron density obtained by the electron simulation (L=8 mm, r_1=19 mm, r_2=25 mm): (b) in the case of "reflection", • :with Eq. (38), and △: with Eq. (39), (c) with Eq. (40), • : in the case of "reflection", and △: in the case of "secondary-electron emission" (the radial electric field at the outer wall is also plotted), and (d) with Eq. (40) in the case of "loss".

$$\phi = \left[\phi_0 + \bar{\phi}_{1m} \cos(k_\theta \bar{r}\theta - \omega t)\right] \sin\left(\frac{r - r_1}{r_2 - r_1}\pi\right), \quad (40)$$

where $\bar{\phi}_{1m}$ is the amplitude of the space potential oscillation at $r = \bar{r}$. They differ in their gradient attributable to walls : Eq. (38) causes no radial electric field, Eq. (39) dose the constant radial field and an oscillating azimuthal field, and Eq. (40) dose oscillating radial and azimuthal fields. As seen in Fig. 7(b) and (c), the same spatial periodicity of the density as in the previous simulation is observed only when the radial electric field fluctuates. Figure 7(c) and (d) show the effect of the interaction between electrons and wall surfaces. The following cases were considered: 1) reflection—all electrons arriving at the wall surface are reflected by the wall sheath, changing the direction of their velocities, 2) secondary-electron emission — an electron is emitted whenever an electron reaches the wall(δ=1), and 3) loss— all of them are lost on the surface; no secondary-electron is emitted(δ=0). In the case of "loss", the periodicity is more obscure because the electric field cannot keep affecting their trajectories for as long time as in other cases. Figure 8 shows the results on the same condition as Fig. 7(c). The amplitude of the oscillation component of the azimuthal velocity $|\bar{v}_{elx}|$ is bigger than the result based on the fluid equation; it is the same order of magnitude as that seen in Fig. 6. The phase difference between the velocity and the density agrees with that estimated from Eq. (30). Though it is found that the interaction with wall and the radial field have influence on the azimuthal variation of the electron properties, it has not become possible to predict the magnitude of velocity perturbation without simulation. The further study is therefore required as to this phenomenon.

The relation among electron density, ion density,

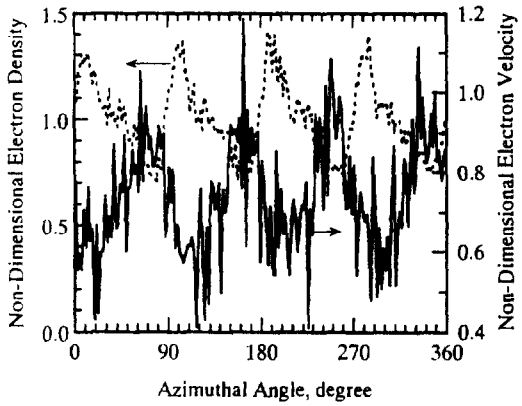

Fig. 8 Results of the electron simulation on the same condition as in Fig. 7(c)(in the case of "reflection").

and resulting space potential is governed by the linearized Poisson equation:

$$\Delta\phi_1 = -\frac{e}{\varepsilon_0}(n_{i1} - n_{e1}) \tag{41}$$

Referring to Eq. (20), this becomes

$$-k_x{}^2\bar{\phi}_1 = -\frac{e}{\varepsilon_0}|\bar{n}_{i1}|[\exp(-i\alpha_i) - \exp(-i\alpha_e)]. \tag{42}$$

Thus, two phases should satisfy the relationship:

$$\alpha_i + \alpha_e = (2n-1)\pi \quad n = 1,2,\cdots, \tag{43}$$

which is recognized in Fig. 5.

Substituting Eqs. (27) and (30) into Eq. (20), $|\bar{n}_{e1}|$ can be estimated. With the frequency and the space potential perturbation read in Figs. 3 and 4, it becomes 0.1 in the dimensionless unit, which has the same order as the simulation result as seen in Fig. 6.

Moreover, these equations allow us to get the following equation for the wave frequency:

$$\begin{aligned}&\omega^4 + \left[(2\partial_y v_{i0y})^2 - P - 2Q\right]\omega^2 \\ &+ \left(2k_x v_{e0x}P - 4\partial_y v_{i0y}R\right)\omega - P(k_x v_{e0x})^2 + Q^2 + R^2 = 0\end{aligned} \tag{44}$$

where

$$\begin{aligned}&P \equiv \frac{n_{i0}ek_x\bar{\phi}_1}{n_{e0}|\bar{v}_{ex1}|m_i}, Q \equiv (\partial_y v_{i0y})^2 + \omega_{ci}{}^2, \\ &R \equiv \omega_{ci}k_x v_{i0y}.\end{aligned} \tag{45}$$

The solution of this equation can be approximately expressed as follows:

$$\omega = \frac{-P \pm \sqrt{P^2 - 4\left[(\partial_y v_{i0y})^2 - Pk_x v_{e0x}\right]}}{2} \quad \text{for } \omega < k_x v_{e0x}, \tag{46}$$

$$\omega = \frac{P \pm \sqrt{P^2 + 4\left[(\partial_y v_{i0y})^2 - Pk_x v_{e0x}\right]}}{2} \quad \text{for } \omega > k_x v_{e0x}. \tag{47}$$

Entering the wave number $k_x = 4/\bar{r}$, the amplitude of the electron azimuthal velocity observed in the simulation, $|\tilde{\bar{v}}_{e1x}|$ =0.1-0.3, and other conditions into Eq. (44), the period is calculated to be in the range from $370/\omega_{pe}$ to $710/\omega_{pe}$, which is close to the simulation result. From Eqs. (44) - (47), it is indicated that this wave frequency dose not drastically depends on the plasma density, if neither the potential perturbation nor the wave number changes. The above period corresponds to the frequency from 2.5 to 4.8 MHz; the frequency is estimated to be about 3-5 MHz on the condition that B_z=0.1 T, V_a=100-300 V.

Referring to these discussions, it is thought that the fluctuation in Fig. 3-6 originates in the difference between electron and ion behavior: electrons are influenced by the magnetic field, oscillation of the radial electric field, and the interaction with the wall besides the azimuthal electric field, while the ion motion is mainly dominated by the applied axial field and the oscillating azimuthal field.

Particle Simulation of Plasma in the Oscillating Field

The particle simulation of plasma was carried out again to investigate the effect of the oscillating electric field on the electron transport. The equilibrium part of the space potential ϕ_0 is self-consistently determined, while its oscillating part ϕ_1 is given by the equations:

$$\phi_1 = \bar{\phi}_{1m}\sin\left(\frac{r-r_1}{r_2-r_1}\pi\right)\cos(k_\theta\bar{r}\theta - \omega t) \quad (0 \le z < L),$$

$$\phi_1 = \bar{\phi}_{1m}\sin\left(\frac{r}{2\bar{r}}\pi\right)\cos(k_\theta\bar{r}\theta - \omega t) \quad (L \le z). \tag{48}$$

These are used when the variation with angle and with time is needed without solving the Poisson equation three-dimensionally. Figures 9 and 10 show obtained space potential distributions in the r-z plane. When the channel walls are insulated, in other words, the wall

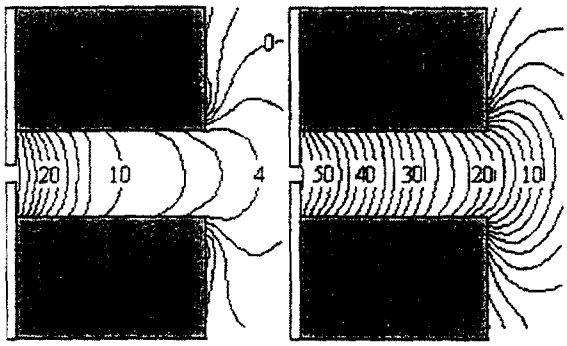

(a) (b)

Fig. 9 Space potential distributions (in the dimensionless unit) obtained by the particle simulation when the channel walls are insulated (L=8 mm, r_1=25 mm, r_2=30 mm, γ =0.2, K_n =0.4, and δ=0.6): (a) with an oscillating electric field ($\tilde{\bar{\phi}}_{1m}$ =6, $k_\theta\bar{r}$ =4, $\tilde{\omega}$ =2π/400) and (b) without an

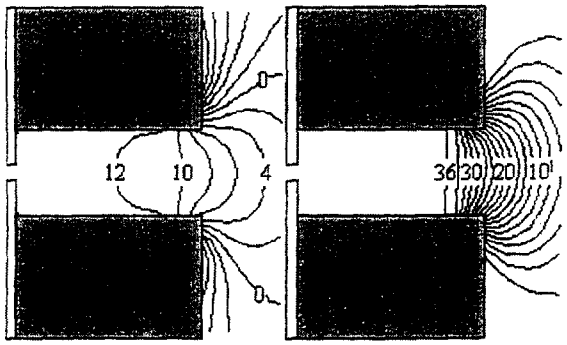

Fig. 10 Space potential distributions (in the dimensionless unit) obtained by the particle simulation when the channel walls are the anodes (L=8 mm, r_1=25 mm, r_2=30 mm, γ =0.2, K_n =0.4, and δ=0.6): (a) with an oscillating electric field ($\tilde{\phi}_{1m}$ =6, $k_\theta \bar{r}$ =4, $\tilde{\omega}$ =2π/400) and (b) without an oscillating field.

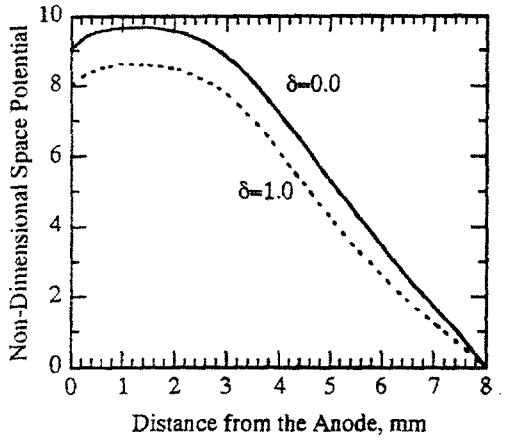

Fig. 11 Effect of the secondary-electron emission on the space potential distribution at $r = \bar{r}$ ($\bar{\phi}_{1m} = 0$, L=8 mm, r_1=19 mm, r_2=25 mm, γ=0.3, K_n =0.3).

potential is floating, the electric field is formed throughout the channel (Fig. 9). On the contrary, no electric field is formed at the depth of the channel when the walls are the anodes (Fig. 10). This result accounts for the difference in the channel length between the stationary plasma thrusters and anode layer thrusters. As seen in these figures, the axial electric field induced in the stable and azimuthally uniform plasma is stronger than that in the fluctuating plasma, although the discharge currents are chosen to be equal. This fact indicates that the fluctuation raises the electron mobility normal to the magnetic field.

Figure 11 shows an effect of the secondary-electron emission yield δ on the axial distribution of the space potential. An increase in δ accompanies a slight decrease in the axial electric field, in other words, an increase in the electron mobility.

Conclusions

The plasma fluctuation and its effect on the electron behavior in a Hall thruster were investigated using the particle simulation and the analysis based on the equation of continuity and the fluid equation of motion. From the results, it was suggested that the plasma fluctuation found in the simulation is due to the difference between electron and ion motion in the azimuthal direction. Moreover, it was found that the azimuthal variation of electron properties is influenced by the oscillation of the radial electric field and the interaction with wall surfaces besides the azimuthal electric field. The results of the particle simulation also showed that the oscillation of electric fields contributes to an increase in the electron mobility normal to the magnetic field more than the secondary-electron emission from the wall surfaces.

References

1. Bugrova, A. I., Morozov, A. I. and Kharchevnikov, V. K.," Wall-Conductivity Effects in the Channel of a Closed-Drift-Circuit Plasma Accelerator," *Sov. Tech. Phys. Lett.*, Vol. 9, No. 1, January 1983, pp. 1, 2.

2. Yoshikawa, S. and Rose, J., "Anomalous Diffusion of a Plasma across a Magnetic Field," *Phys. Fluids*, Vol. 5, No. 3, March 1962, pp. 334-340.

3. Popov, Y. S. and Zolotaikin, Y. M., "Effect of Anomalous Conductivity on the Structure of the Anode Sheath in a Hall-Current Ion Source," *Sov. J. Plasma Phys.*, Vol. 3, No. 2, March-April 1977, pp. 210-213.

4. Hirakawa, M. and Arakawa, Y., "Plasma Particle Simulation in Cusped Ion Thrusters," IEPC-93-242, 23rd International Electric Propulsion Conference, Seattle, WA, September 1993.

5. Hirakawa, M. and Arakawa, Y., "Particle Simulation of Plasma Phenomena in Hall Thrusters," *Proc. of the 24th International Electric Propulsion Conference*, Moscow, Russia, September, Vol. 2, 1995, pp. 1137-1144.

6. Baranov, V. I., et al., "New Conceptions of Oscillation Mechanisms in the Accelerator with Closed Drift of Electrons," *Proc. of the 24th International Electric Propulsion Conference*, Moscow, Russia, September, Vol. 1, 1995, pp. 344-351.

7. Baranov, V. I., et al., "Theory of Oscillations and Conductivity for Hall Thruster," AIAA 96-3192, 32nd AIAA/ASME/SAE/ASEE Joint Propulsion Conference, July 1996, Lake Buena Vista, FL.